# Fatigue Behavior in Ceramics

TAKASHI KAWAKUBO

Toshiba Corporation, Research and Development Center, Komukai Toshiba-cho 1, Saiwai-ku, Kawasaki 210 Japan

ABSTRACT

Static and cyclic fatigue behavior of different ceramics were investigated at room temperature. Specimens with an indentation-induced flaw at the center were tested under a static or cyclic load applied by four-point bending. Effects of loading frequency and stress ratio were examined. All ceramics showed to be susceptible to fatigue failure. Comparing static and cyclic fatigue behavior demonstrated a large fatigue acceleration by cyclic loading in many types of ceramics, such as silicon nitride and TZP ceramics. The cyclic loading effect on fatigue were classified into two categories, i.e., an intergranular cracking and a stress-induced transformation. It was suggested that the acceleration is related to the nonlinear microfractures in the process zone, such as crack branching, deflection and multiple cracking of intergranular cracking, and a stress-induced transformation.

## INTRODUCTION

Recently, numbers of advanced ceramics have been developed for engineering uses. Advanced ceramics are promising for wide applications due to their superior high-temperature strength and corrosion and wear resistances. For any engineering applications, it is indispensable to evaluate the fatigue behaviors under various loading modes.

The present study focuses on the mechanical fatigue behavior of oxide and non-oxide ceramics. Particularly, the determination of controlling parameters for fatigue life was emphasized by comparing static and cyclic fatigue life.

## CONVENTIONAL FATIGUE THEORY

Conventional fatigue theory[1,2] consists of linear-elastic fracture mechanics expressed by Eq.(1) and fully time-dependent fatigue crack growth assumption expressed by Eq.(2).

$$K = Y\sigma_a\sqrt{\pi a} \tag{1}$$

$$da/dt = AK^n \tag{2}$$

Where $K$ =stress intensity factor, $Y$ =shape parameter, $\sigma_a$=applied stress, $a$ =crack length, $t$ =time, and $A, n$ =constants. Initial and final crack lengths are denoted by $a_i$ at $t$ =0 and $a_f$ at $t_f$, respectively. The applied stress is expressed by $\sigma_a = \sigma_0 f(t)$, where $(0 \leqq f(t) \leqq 1)$. Integrating Eq.(2) yields

$$a_f^{(2-n)/2} - a_i^{(2-n)/2} = [2-n/2][AY^n\pi^{n/2}\sigma_0^n]\int_0^{t_f}[f(t)]^n dt \tag{3}$$

Static fatigue life ($t_f$) is obtained from Eq.(4) by the fact that $a_i^{(2-n)/2} \gg a_f^{(2-n)/2}$ for the exponent $n$ is as large as several tens, and

$f(t)=1$ for static loading;

$$t_f \fallingdotseq [2/(n-2)][Y^n \pi^{n/2} A a_i^{(n-2)/2} \sigma_0^n]^{-1} \quad (4)$$

In cyclic test with a period $\lambda$, cyclic fatigue life can be obtained as well as static fatigue life;

$$t_f \fallingdotseq [2/(n-2)][Y^n \pi^{n/2} A a_i^{(n-2)/2} \sigma_0^n]^{-1} \lambda \{\int_0^\lambda [f(t)]^n dt\}^{-1} \quad (5)$$

The ratio of fatigue lifetimes of static to cyclic tests, $h$, $\{=(1/\lambda)\int_0^\lambda [f(t)]^n dt\}$ can be easily obtained numerically using computer.

## EXPERIMENTAL

Materials studied are seven different types of ceramics; alumina I and II, tetragonal zirconia polycrystal (TZP), zirconia-alumina, $Pb(Zr,Ti)O_3$ (PZT), silicon carbide, and silicon nitride. The purity of alumina I and II is 99.5% and 99.99%, respectively. TZP is partially stabilized by 3 mol% yttria doping. zirconia-alumina contains 20Wt% alumina and 3mol% yttria doped zirconia. Silicon carbide is beta-type sintered with boron and carbon. Silicon nitride is sintered with about 10% of additives of alumina, yttria etc.

Static and cyclic fatigue tests are conducted using rectangular bar specimens with four-point-bending configuration, the details of loading apparatus have been reported elsewhere[3]. All tests are conducted at room-temperature in air with relative humidity of 50% to 80%. A sinusoidal wave of the frequency of 10Hz and the stress ratio of 0 (zero-tension) is employed for standard cyclic fatigue test. For TZP and Alumina II, effects of frequency of 0.01 to 10 Hz and stress ratio of -1 to 1 are examined. In both static and cyclic fatigue specimens,

microcracks are introduced by Vickers indentation with load of 9.8 to 98N prior to fatigue tests.

Fracture surfaces of the specimens are examined by SEM (scanning electron microscope) after gold vacuum vapor deposition. Some specimens were immersed in a solution of hydrochloric and hydrofluoric acids to remove a glassy phase on fracture surfaces. X-ray diffraction is also applied to fracture surfaces of TZP and zirconia-alumina. Tetragonal and monoclinic phase fractions are determined in the overall fracture surface.

## RESULTS

All ceramics showed static and cyclic fatigue. Figures 1 to 3 show flexural strength and fatigue life for alumina Ⅱ, TZP and silicon nitride. Regression lines for static and cyclic data, and the predicted cyclic fatigue line from static data using $h$ value were drawn in the figures. A large degradation in fatigue strength was observed for these ceramics. The cyclic fatigue strength of TZP at $10^7$ cycles is about one-third of the flexural strength. Figure 4 summarizes the crack growth exponent $n$ of static and cyclic fatigue, which is defined by the inverse of slope of the stress-failure time curve. Examined ceramics showed increasing fatigue strength degradation in this order; silicon carbide, PZT, silicon nitride, alumina I (99.5%), alumina Ⅱ (99.99% purity), zirconia-alumina and TZP. Comparing the measured and the predicted cyclic fatigue strengths, only minor differences were observed in silicon carbide and alumina I, while cyclic strength was

much smaller than the predicted strength in alumina II, zirconia-alumina, TZP, PZT and silicon nitride. In these ceramics, the exponent $n$ was different between static and cyclic fatigue data. In addition, the scatter in cyclic fatigue life data for silicon nitride was much smaller than that in the static case.

Effects of loading frequency and stress ratio (minimum stress/maximum stress) are examined in order to study the cycle/time dependence. Figures 5 and 6 show time-based cyclic fatigue life at a fixed maximum stress and different frequencies of 0.01 to 10 Hz for alumina II and TZP, respectively. In the figures, fully time-dependent failure should be represented by a horizontal line, and fully cycle-dependent failure by a line with a slope of -1. The regression line for both ceramics has a slope of about -0.4, which indicates intermediate dependence with time and loading cycle. Figures 7 and 8 show fatigue lifes at different stress ratios and fixed frequency of 10 Hz for alumina II and TZP. Predicted lifetime from static data is also shown in the figures using the conventional fatigue theory. Decreasing the stress ratio (sustained → fluctuated → reversed stress), fatigue life decreased while the predicted life increased.

Macroscopic fractography showed semicircular fatigue cracked regions except for alumina I and silicon carbide. Fracture toughness, estimated from the crack size and applied load, was identical for each ceramics in static and cyclic loading. Microscopic fractography revealed different cracking modes depending on the ceramics. There seemed fracture mode transitions from fatigue to fast fracture surface

for TZP (predominantly transgranular cracking to mixed mode of cracking) and alumina Ⅱ (intergranular to mixed). Alumina Ⅰ, zirconia-alumina, PZT and silicon nitride showed a failure dominated by intergranular cracking, and silicon carbide showed transgranular cracking both in fatigue and fast fractured portions.

X-ray diffraction on TZP and zirconia-alumina specimens showed that little monoclinic phase was detected in the static fatigue specimen, although 10 to 30% of transformation from tetragonal to monoclinic was observed for the overall cyclic fatigue specimens.

## DISCUSSION

Current experimental investigation clarified that conventional fatigue theory, where the crack growth rate is time-dependent only, is applicable to limited types of ceramics, and that large fatigue crack growth acceleration due to cyclic loading was observed in many types of ceramics, such as alumina Ⅱ, TZP and silicon nitride. Table 1 summarizes the microstructure, crack morphology, exponent $n$ with regression coefficient $r$, and a degree of cyclic loading acceleration. Ceramics, which showed accelerated cyclic fatigue, are considered to be classified into two types.

The first type is seemed to be related to an intergranular cracking and the fracture surface roughness. Schematic illustrations for observed crack morphology are shown in Fig.9. Silicon carbide with flat transgranular cracking had no accelerated fatigue failure under cyclic loading. On the other hand, silicon nitride, which showed

intergranular cracking of elongated columnar crystals microstructure, exhibited much higher cyclic fatigue susceptibility than static fatigue.

The second type is characterized by enhanced phase transformation by cyclic loading, observed in TZP and zirconia-alumina. Partially stabilized tetragonal phase is known to transform to monoclinic phase by stressing or by low temperature annealing under presence of moisture or water. The cyclic stress gives rise to much enhanced phase transformation at the crack tip than the static stress does.

The enhanced fatigue degradations in ceramics mentioned above were considered to be corresponding with the nonlinear fracture process of ceramics [4]. Even in ceramics, process zone can be formed at the crack tip, where nonlinear fracture takes place. This process zone comprises microcracking, phase-transformation, dislocation in crystal, and the size depends strongly on ceramic microstructures. It should be noted that crack tip process zone can be formed by intergranular cracking associated with crack branching, deflection and multiple cracking, and also by stress-induced transformation. The process zone formation causes stress hysteresis in cyclic loading, and fatigue crack growth acceleration results from dispersed energy during the cyclic process.

## CONCLUSIONS

All ceramics examined showed static and cyclic fatigue at room temperature. Comparing static and cyclic fatigues, a large fatigue crack growth acceleration by cyclic loading was observed in alumina II

(99.99% purity), zirconia-alumina, TZP, and silicon nitride, although the fatigue life was similar in both cases for silicon carbide and alumina I (99.5% purity). Macroscopic fractography showed semicircular fatigue cracked regions in several ceramics. Microscopic fractography revealed different cracking modes depending on the ceramics. There seemed fracture mode transition from fatigue to fast fracture for TZP (predominantly transgranular to mixed type of cracking) and alumina II (intergranular to mixed). X-ray diffraction on TZP and zirconia-alumina specimens showed accelerated transformation from tetragonal to monoclinic for cyclic fatigue specimens. Fatigue acceleration by cyclic loading is classified into two categories, i.e., an intergranular cracking and a stress induced transformation. It is suggested that these accelerations are considered to be a result of nonlinear microfracture under cyclic loading in the process zone, such as crack branching, deflection and multiple cracking effects in intergranular cracking, and a stress-induced phase transformation accompanied by microcracking.

References

1. S.M.Wiederhorn,"Subcritical Crack Growth in Ceramics"; pp.613-46 in Fracture Mechanics of Ceramics, Vol.2, Edited by R.C.Bradt et al. Plenum Press, New York, 1973.

2. A.G.Evans and E.R.Fuller, "Crack Propagation in Ceramic Materials under Cyclic Loading Conditions," Metall.Trans., 5, 27-33 (1974).

3. T.Kawakubo and K.Komeya, "Static and Cyclic Fatigue Behavior of a

Sintered Silicon Nitride at Room Temperature," J.Am.Ceram.Soc., 70, 400-05 (1987).

4. M.Sakai,"Nonlinear Fracture Phenomena"; Chp.7 in Evaluation of Dynamic Properties in Ceramics, Edited by T.Nishida et al. Nikkankogyo Shinbunsha, Tokyo, 1986, in Japanese.

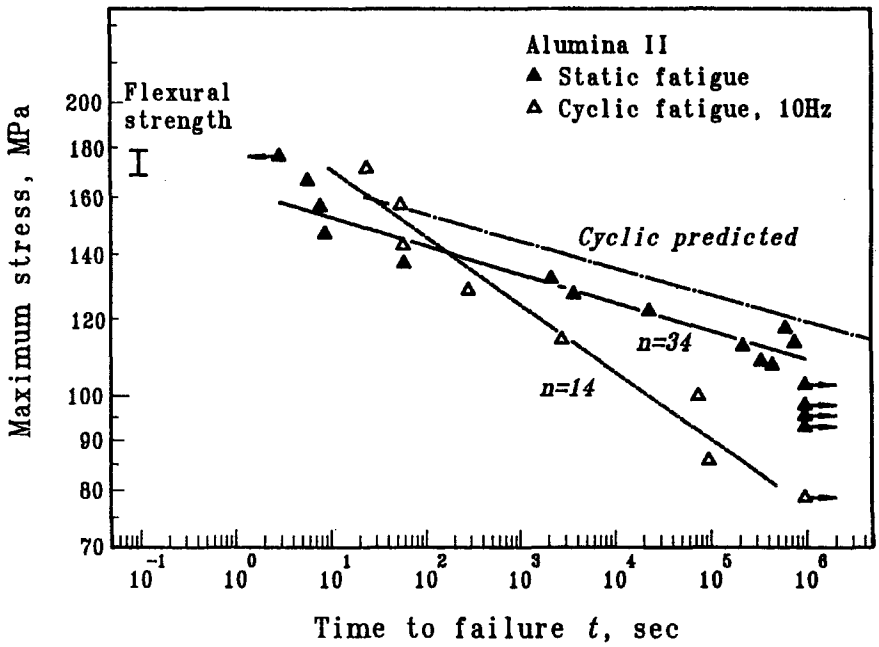


Figure 1 Static and cyclic fatigue strength for alumina Ⅱ at room temperature air.

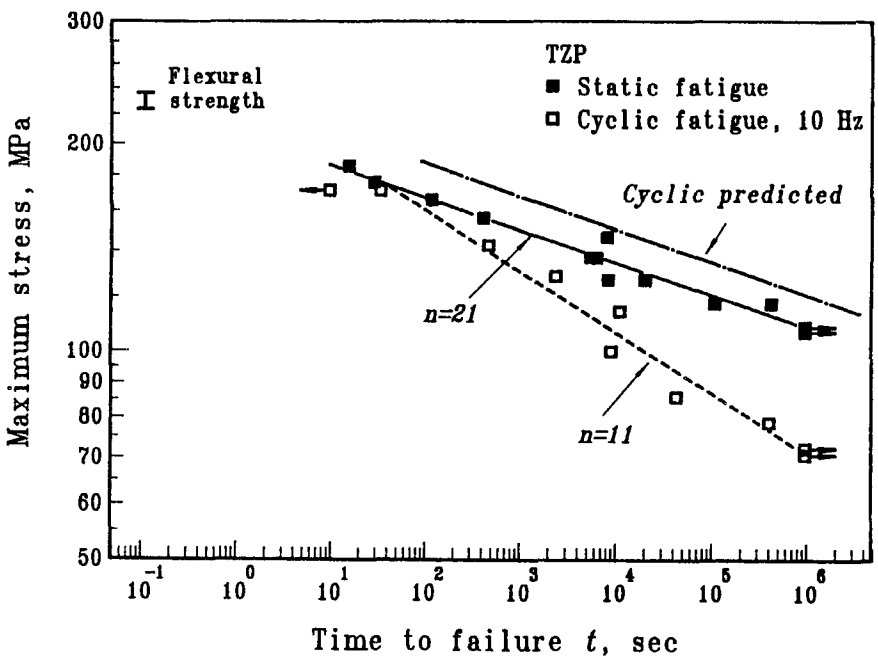


Figure 2 Static and cyclic fatigue strength for TZP at room temperature air.

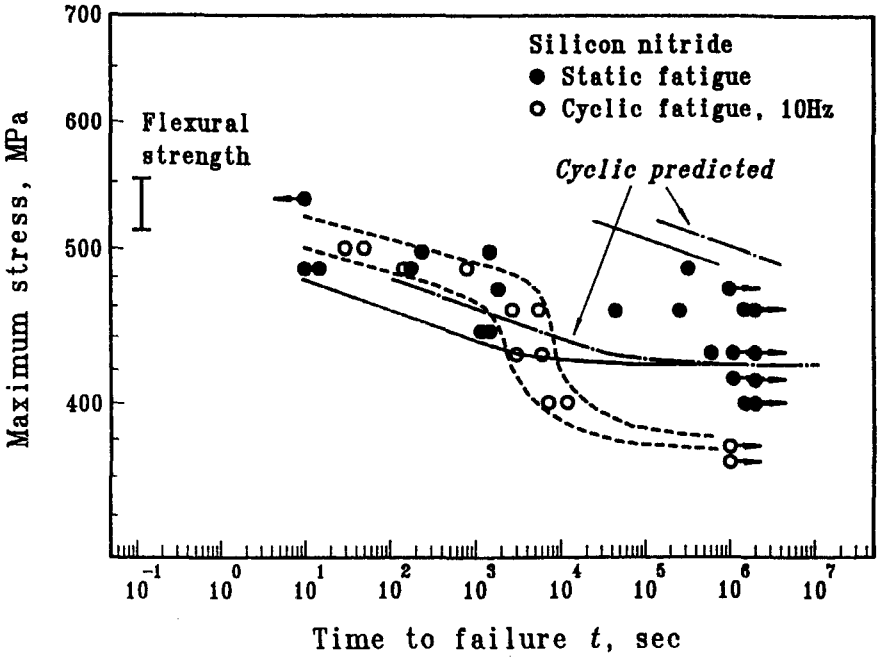


Figure 3 Static and cyclic fatigue strength for silicon nitride at room temperature air.

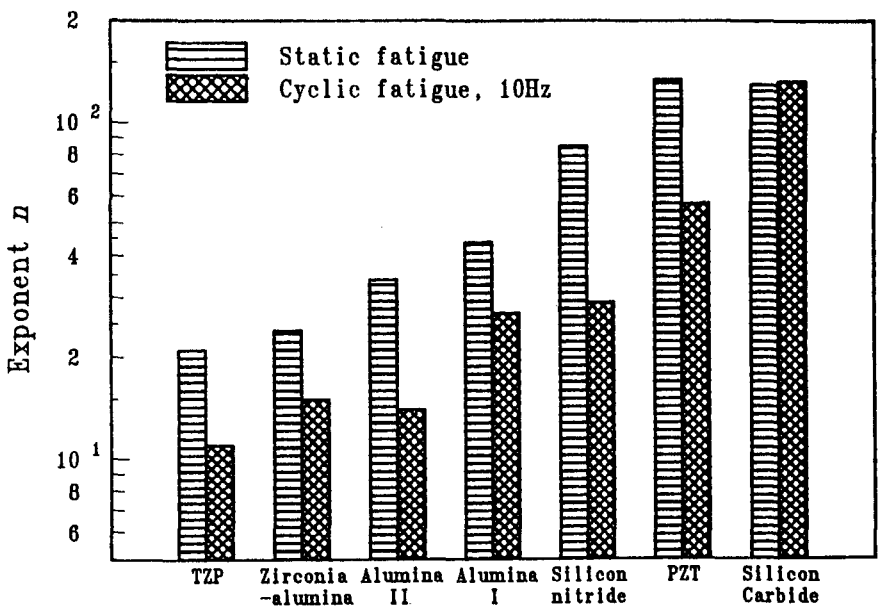


Figure 4 Crack growth exponent n in static and cyclic fatigue.

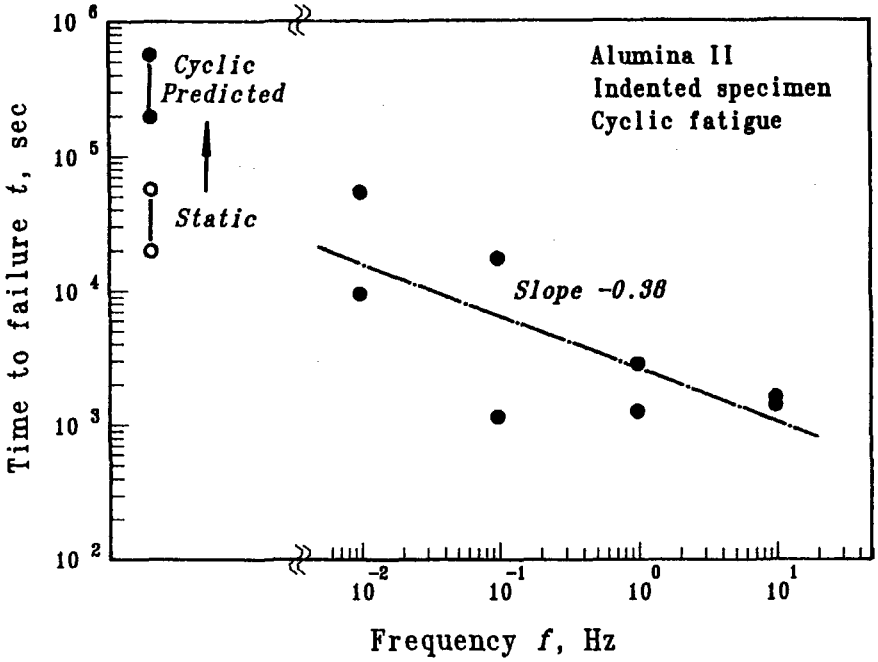


Figure 5 Effect of frequency on cyclic fatigue life for alumina Ⅱ.

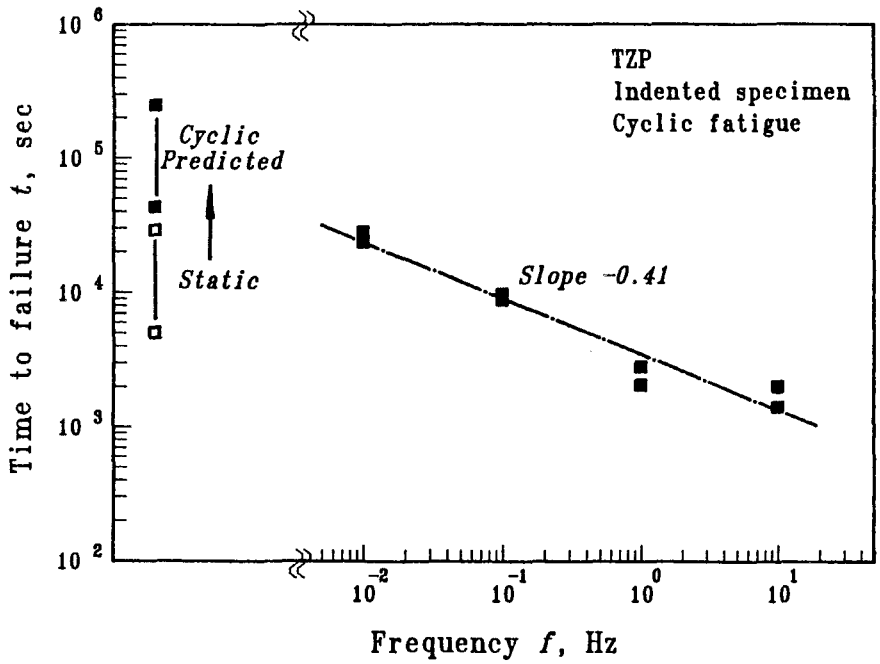


Figure 6 Effect of frequency on cyclic fatigue life for TZP.

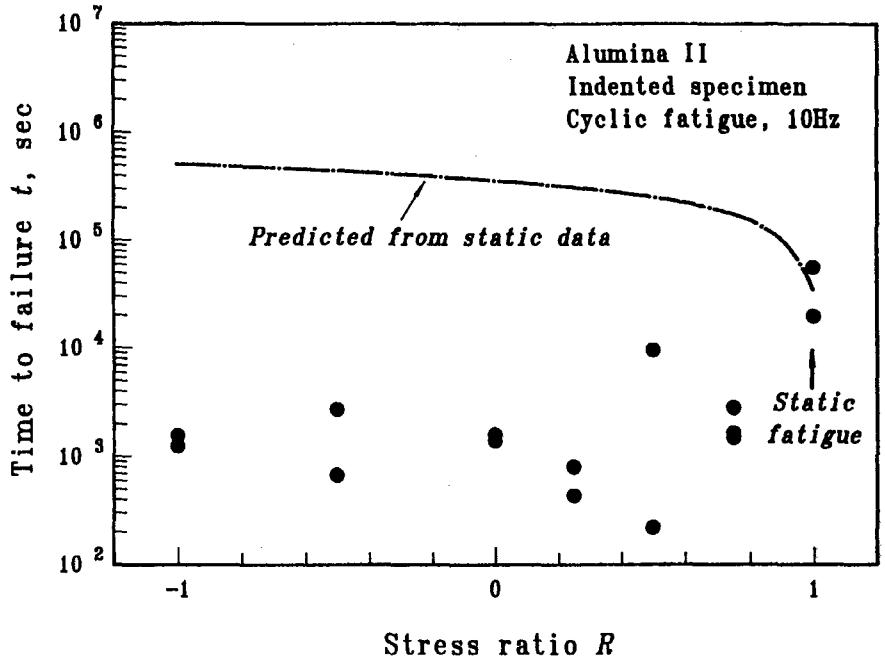


Figure 7 Effect of stress ratio on cyclic fatigue life for alumina Ⅱ.

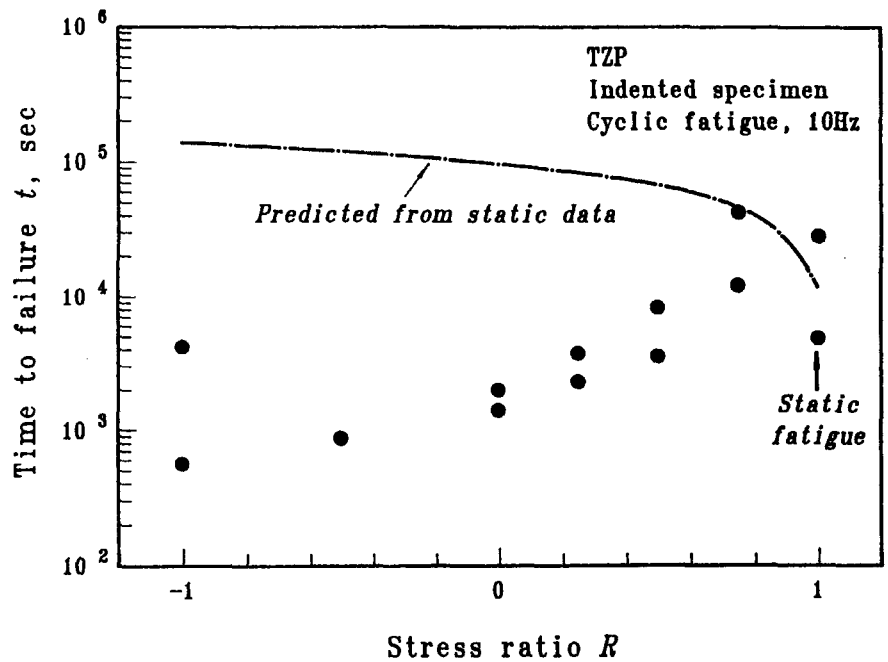


Figure 8 Effect of stress ratio on cyclic fatigue life for TZP.

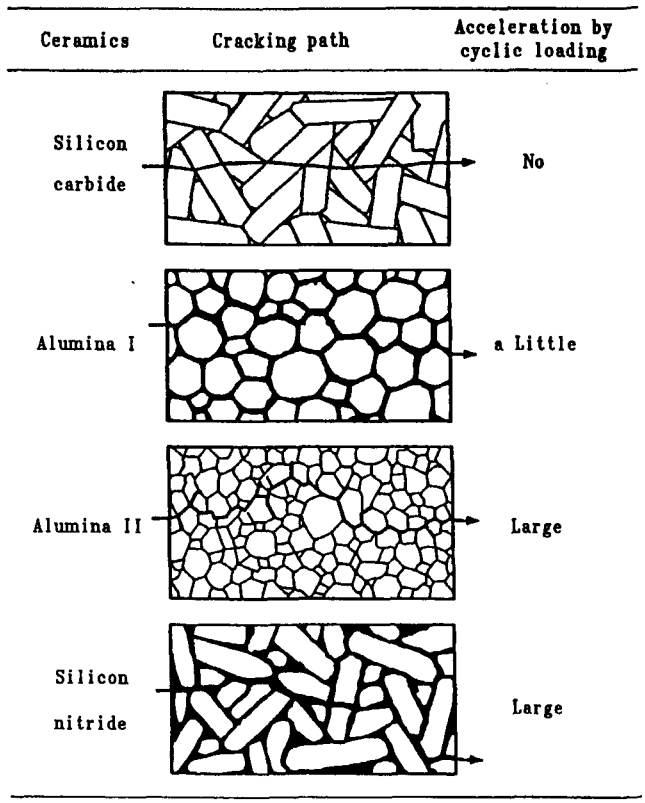


Figure 9 Schematic illustration for fatigue crack growth path.

TABLE 1 Summary of fatigue degradation and cracking morphology.

| Material | Crystal shape | Crystal size in $\mu m$ | Cracking morphology | | | n-value/r-value | | Acceleration by cyclic loading |
|---|---|---|---|---|---|---|---|---|
| | | | Stat. fat. | Cyc. fat. | Fast frac. | Stat. fat. | Cyc. fat | |
| Silicon carbide | Columnar | 2-3 $\phi$ | T. G. | T. G. | T. G. | 129/0.68 | 132/0.62 | No |
| PZT | Granular | 2-5 | Mixed | Mixed | Mixed | 134/0.82 | 57/0.87 | Medium |
| Alumina I | Granular | 1-20 | I. G. | I. G. | I. G. | 44/0.80 | 27/0.73 | Little |
| Alumina II | Granular | 2-10 | I. G. | I. G. | Mixed | 34/0.96 | 14/0.97 | Large |
| Silicon nitride | Columnar | ~1 $\phi$ | I. G. | I. G. | I. G. | 85/0.67 | 29/0.87 | Large |
| 3Y-zirconia | Granular | 0.5-1 | Mixed | Mixed* | I. G. | 21/0.97 | 11/0.97 | Large |
| zirconia-alumina | Granular | 0.5-1.5 | Mixed | Mixed* | Mixed | 24/0.97 | 13/0.95 | Medium |

* Transformation from tetragonal to monoclinic was detected